



# Efficient diffeomorphic metric image registration via stationary velocity

Xianfeng Yang<sup>a,\*</sup>, Jian Yang<sup>b</sup>

<sup>a</sup> Key Laboratory of Intelligent Perception and Systems for High-Dimensional Information of Ministry of Education, School of Computer Science and Engineering, Nanjing University of Science and Technology, Nanjing, 210094, PR China

<sup>b</sup> Jiangsu Key Laboratory of Image and Video Understanding for Social Security, School of Computer Science and Engineering, Nanjing University of Science and Technology, Nanjing, 210094, PR China

## ARTICLE INFO

### Article history:

Received 7 August 2018

Received in revised form

26 November 2018

Accepted 28 November 2018

Available online 2 December 2018

### Keywords:

Diffeomorphic mapping

Brain registration

Large deformation

Stationary velocity

Non-stationary velocity

Mean value theorem

## ABSTRACT

Diffeomorphic image registration is a fundamental tool for MRI analysis, and fast growing image data demand highly efficient registration methods. Stationary velocity based method has much faster speed than non-stationary one in producing diffeomorphism, but how to achieve validity for large deformation while keeping its efficiency remains to be solved. To this end, we have proposed a new simplified model for optimal stationary velocity by representing temporal integration form of transformation variation via a single point model, e.g. the middle time point, according to mean value theorem and smoothness of transformation. This model can maintain the same registration accuracy as integral model but reduce the time cost a lot. It also shows as a better strategy than first order approximation model for large deformation mapping. Comparative study has also been conducted between this method and non-stationary approach on both synthesized and real brain images, and this approach demonstrated comparable whole brain mapping accuracy with much faster speed. Results showed efficacy of this approach in reducing complexity of stationary velocity based diffeomorphic registration while achieving validity for large deformation.

© 2018 Elsevier B.V. All rights reserved.

## 1. Introduction

Diffeomorphic image registration is essential for many brain imaging analysis tasks, such as anatomical variability analysis [1–3], atlas building and brain segmentation [4,5], functional magnetic resonance image (fMRI) analysis [6] and so on. Diffeomorphism (one-one and smooth mapping) under large deformation can be achieved by temporally integrating smooth vector fields which are usually built as stationary or non-stationary ones. Under non-stationary parameterization, smooth vector fields vary continuously in time, and the solution lies within full diffeomorphism space, which may benefit the mapping of highly complicated cortical structures. The representative method of this kind is the large deformation diffeomorphic metric mapping (LDDMM) [7–12] that has been shown as a powerful approach to characterize anatomical variabilities [13–19]. However, the major drawback of time-varying

approach is its high computational complexity, and many research efforts have been made trying to alleviate this problem [20–23], but their deployment on large scale analysis still needs further work.

On the other hand, stationary velocity parameterization has the advantage of implementation efficiency brought by the scaling and squaring procedure in deformation generation [24–26], and has the ability to achieve satisfactory brain mapping accuracy. Though there have been some stationary approaches proposed, how to achieve good trade-off between accuracy and efficiency is still a research issue worthy of further study. For instance, Hernandez et al. has introduced stationary velocity in context of LDDMM [27], and proposed a 1<sup>st</sup>-order approximation model for optimal velocity that only depends on the end-point deformation information, which showed much faster speed than LDDMM with comparable accuracy in terms of residual. But this model is just valid under small deformation setting, hence its ability to handle large deformation mapping is in question. Some other stationary approaches [28–30] including DARTEL in SPM package adopted integral model of optimal velocity to achieve validity under large deformation setting. Computation of this integral model relies on deformations uniformly sampled in time interval [0,1], which is similar to the operations in time-varying approach, so efficiency brought by the

\* Corresponding author at: School of Computer Science and Engineering, Nanjing University of Science and Technology, Xiao Ling Wei Str. 200, Nanjing, Jiangsu Province, 210094, China.

E-mail address: [yangxianfeng@njjust.edu.cn](mailto:yangxianfeng@njjust.edu.cn) (X. Yang).

scaling and squaring procedure is compromised, and heavy computational load is incurred in velocity gradient computation, and this problem becomes more protrude for large size volumes.

Aiming to find better solution to improve efficiency of stationary parameterization while achieving its validity for large deformation, we have proposed a new simplified model for optimal velocity which exhibits the same accuracy as the integral model but increases speed significantly. Not only to provide efficient method to align brain anatomy, this work is also targeted to accelerate large scale nonlinear brain manifold analysis. Previous work showed that diffeomorphic metric mapping via stationary velocity had advantage in high order shape metric approximation [30], which can benefit manifold analysis of highly nonlinear brain shapes, so acceleration of the stationary approach will be of great value for large scale brain manifold analysis. Besides validating the proposed model, we will also conduct comprehensive comparison between stationary and non-stationary approaches regarding their whole brain registration accuracy and speed, regularized energy, resulting deformation fields and velocity fields. Such comparative study allows us to better understand the behaviors of the two parameterizations in high dimensional diffeomorphic mapping. To our knowledge, such study is still scarce for image registration.

In the remaining part of the paper, we will first describe in detail the proposed method in Section 2, and in Section 3 present its results on both synthesized images and real brain data, as well as the comparison with other brain registration methods, including the stationary approach by first order approximation [27] and integral model, LDDMM [7], as well as diffeomorphic demons [26,31]. Discussion of the methodology is given in Section 4, and conclusion of this work is drawn in Section 5.

## 2. Methodology

This section will present the theoretical basis of diffeomorphic metric mapping, variational derivation of the optimal stationary velocity and the image registration algorithm.

### 2.1. Theoretical basis of diffeomorphic metric mapping

Stationary velocity field  $v$  keeps fixed *w.r.t.* time, and the transformation  $\phi_t^v$  driven by  $v$  satisfies the following differential equation,

$$\frac{\partial \phi_t^v(\mathbf{x})}{\partial t} = \mathbf{v}(\phi_t^v(\mathbf{x})), \quad t \in [0, 1] \quad (1)$$

where  $\phi_1^v$  is the desired end-point transformation. The deformation path generated by (1) is a one-parameter sub-group in diffeomorphism space and the following scaling and squaring procedure holds:

$$\phi_{2/N} = \phi_{1/N} \circ \phi_{1/N} \quad \dots$$

$$\phi_{1/2} = \phi_{1/4} \circ \phi_{1/4}$$

$$\phi_1 = \phi_{1/2} \circ \phi_{1/2}$$

Based on this procedure, if the time interval  $[0, 1]$  is divided into  $N$  steps, only  $\log_2 N$  compositions are needed to compute  $\phi_1$ , hence implementation of stationary parameterization becomes very efficient.

Under stationary velocity setting, image registration is formulated as minimizing the following energy functional,

$$\mathbf{E}(\mathbf{v}) = \mathbf{E}_r + \mathbf{E}_d = \gamma_1 \|\mathbf{v}\|_V^2 + \int_{\Omega} (\mathbf{I}_0 \circ \phi_1^v - \mathbf{I}_1)^2 d\mathbf{x} \quad (2)$$

where data term  $E_d$  is defined as the sum of squared difference (SSD) of images,  $I_0$  is the moving image, and  $I_1$  the fixed one for one-side matching. The regularization term  $E_r$  is defined as Sobolev norm of vector field as adopted in LDDMM that can enforce smoothness of transformation, which is computed by  $\|\mathbf{v}\|_V^2 = \langle \mathbf{v}, \mathbf{v} \rangle_V = \langle L^* L \mathbf{v}, \mathbf{v} \rangle_2$ , where  $L$  is a linear differential operator, and  $L^*$  its adjoint operator,  $L^* L \mathbf{v}$  is the dual space of  $\mathbf{v}$  called momentum space. In this paper,  $L = \gamma \mathcal{I} d - \alpha \Delta$ , where  $\Delta$  is the Laplacian operator,  $\gamma, \alpha > 0$ , and this operator is self-adjoint  $L^* = L$ .  $\gamma_1$  is the regularization parameter controlling the trade-off between matching residual and transformation smoothness.

### 2.2. Variation derivation of optimal stationary velocity

To obtain the gradient of  $E$  that is defined via Frechet derivative  $\nabla_v E(v)$ , we can first compute Gateaux derivative of  $E$  regarding the variation of  $v$ . Given a perturbation  $h$  on  $v$ , Gateaux derivative of  $E_d$  is calculated by,

$$\partial_h \mathbf{E}_d = \int_{\Omega} 2(\mathbf{I}_0 \circ \phi_1^{-v} - \mathbf{I}_1) \nabla \mathbf{I}_0 \circ \phi_1^{-v} \cdot \partial_h \phi_1^{-v} d\mathbf{x} \quad (3)$$

It can be proved that  $\partial_h \phi_1^{-v}$  has the following integral form [30],

$$\partial_h \phi_1^{-v} = \partial_h \phi_{t_0}^v = - \int_0^1 \mathbf{D} \phi_{t_0}^v \mathbf{h}(\phi_{1t}^v) dt \quad (4)$$

In the next, we will simplify this integral form for computational efficiency. Since  $h$  is smooth function, and  $\phi_{1t}^v$  is differentiable in time domain, their composition  $h(\phi_{1t}^v)$  is also continuous in time domain. Moreover,  $\mathbf{D} \phi_{t_0}^v$  is differentiable in time domain, as can be seen by differentiating two sides of Eq. (1) in spatial domain. Based on observations above, the following equation exists according to mean value theorems for definite integrals,

$$\int_0^1 \mathbf{D} \phi_{t_0}^v \mathbf{h}(\phi_{1t}^v) dt = \mathbf{D} \phi_{\xi_0}^v \mathbf{h}(\phi_{1\xi}^v), \quad \xi \in (0, 1) \quad (5)$$

Without prior bias assumption, we estimate  $\xi = 0.5$  here. By this simplification, we can finally get the gradient as follows,

$$\begin{aligned} \nabla_v \mathbf{E}(\mathbf{v}) &= 2\gamma_1 \mathbf{v} - 2(\mathbf{L}^2)^{-1} (\mathbf{I}_0 \circ \phi_{0.5}^{-v} - \mathbf{I}_1 \circ \phi_{0.5}^v) \nabla (\mathbf{I}_0 \circ \phi_{0.5}^{-v}) \\ &\quad | \mathbf{D} \phi_{0.5}^v | \end{aligned} \quad (6)$$

where  $| \mathbf{D} \phi_{0.5}^v |$  is Jacobian determinant. More details of the derivation can be found in the supplemental information online.

Similarly, for two-side matching functional,

$$\mathbf{E}(\mathbf{v}) = \gamma_1 \|\mathbf{v}\|_V^2 + \int_{\Omega} (\mathbf{I}_0 \circ \phi_1^{-v} - \mathbf{I}_1)^2 d\mathbf{x} + \int_{\Omega} (\mathbf{I}_0 - \mathbf{I}_1 \circ \phi_1^{-v})^2 d\mathbf{x} \quad (7)$$

the gradient is,

$$\begin{aligned} \nabla_v \mathbf{E}(v) &= 2\gamma_1 v - 2(\mathbf{L}^2)^{-1} (\mathbf{I}_0 \circ \phi_{0.5}^{-v} - \mathbf{I}_1 \circ \phi_{0.5}^v) \\ &\quad \times (\nabla (\mathbf{I}_0 \circ \phi_{0.5}^{-v}) | \mathbf{D} \phi_{0.5}^v | + \nabla (\mathbf{I}_1 \circ \phi_{0.5}^v) | \mathbf{D} \phi_{0.5}^{-v} |) \end{aligned} \quad (8)$$

Setting (6) and (8) to zero yields the equation of optimal velocity called Euler-Lagrange equation. Thereafter, diffeomorphic metric mapping based on (6) and (8) is referred to as **DMMS**. For comparison, the gradient formula adopting integral form and that adopting the first order approximation [27] are also listed in supplemental information.

### 2.3. Registration algorithm

Based on gradient formula derived above, we have designed the following image registration algorithm.

Initialize velocity field  $v^0 \leftarrow 0$ , and compute initial energy  $E^0$ .

**For**  $k = 1$  to maxiter,

- 1) Compute forward transformation  $\phi_{0.5}^{v^k}$  and backward one  $\phi_{0.5}^{-v^k}$  via scaling and squaring procedure; Calculate Jacobian determinant  $|D\phi_{0.5}^{v^k}|$ , and  $|D\phi_{0.5}^{-v^k}|$  if two side matching is employed.
- 2) Compute velocity gradient  $\nabla_{v^k} E(v^k)$  via Eqs. (6) or (8).
- 3) Perform line search along the velocity gradient, and conjugate method can be used to accelerate the process. Terminate optimization if the following condition is satisfied

$$E^{k-1} - E^k < \epsilon_1(E^0 - E^{k-1}) \quad (9)$$

End

In this algorithm, Jacobian matrix of 3D transformation is computed using forward differentiation,

$$[D(x)]_{ij} = \phi^{(i)}(x + e_j) - \phi^{(i)}(x), \quad i, j = 1, 2, 3 \quad (10)$$

where  $e_j$  is unit vector for  $j$ th axis, and  $\phi^{(i)}$  the  $i$ th component.

In dealing with the boundaries, we have also proposed a strategy different from previous methods. In this approach, the image volume is treated as a closed domain, that is, the left and right boundary points are topologically neighbors, and the same configuration applies to each dimension, which equals to the periodical extension of the image volume. Under this configuration, boundary and interior points will be equally treated in differential operations for image or deformation. This calculation is also compatible with the FFT used to compute velocity field from momentum field or vice versa, because FFT is just based on circular convolution. Moreover, under this configuration it is not necessary for velocity to vanish on boundaries to get compact support, so just few zero paddings are needed to make boundary homogeneous.

## 3. Results

In this section we will first describe the image data used for evaluation of the methods, implementation of the methods and performance measures, then present the results on synthesized and real brain image data.

### 3.1. Experimental settings

#### 3.1.1. Image data

Validity of the proposed method for large deformation mapping was first tested through classical 'Circle-to-C' images (see Fig. 1), and further evaluated on both synthesized and real brain images. Synthesized brain images were drawn from BrainWeb source which include both MRI T1 images (resolution:  $1 \times 1 \times 1 \text{mm}^3$ ) and tissue labels. Six pairs of brain anatomies were randomly chosen for inter-subject registration analysis, and registration based segmentations were compared against the true labels. Real brain images were drawn from publically available image database – ADNI (Alzheimer's disease neuroimaging initiative), including 29 normal elderly subjects (age > 55 years). The skull-stripped volumes were intensity inhomogeneity corrected and resampled to a volume of  $256 \times 256 \times 256$  (resolution:  $1 \times 1 \times 1 \text{mm}^3$ ). One brain image was randomly chosen as the template to register to the rest 28 brains, and registration based segmentations were compared with FreeSurfer segmentations which had wide applications in this field especially for the cortical segmentation based on statistical approach [32].

#### 3.1.2. Method implementation

In this work, we performed comparison between this approach (DMMS) and several other methods, including the stationary approach with integral form of gradient (termed as **stationary-integral**), and stationary approach using first order approximation (termed as **stationary-1<sup>st</sup>-order**), and LDDMM, as well as diffeomorphic demons. LDDMM was implemented according to the algorithms described in Beg, 2005 which adopted semi-Lagrange scheme to integrate time-varying velocity fields, and displacement at each time point was calculated by three iterations to reach convergence. Both stationary approaches and LDDMM were coded in Matlab whose parallel computing toolbox, particularly 'parfor' was utilized to accelerate the computing. Implementation of diffeomorphic demons [31] adopted the publically available Matlab code (<http://www.mathworks.com/matlabcentral/fileexchange/39194-diffeomorphic-log-demons-image-registration>)

#### 3.1.3. Performance measures

Accuracy of registration is measured by Dice of brain tissue segmentation defined as

$$\text{Dice} = \frac{2 |S_A \cap S_B|}{|S_A| + |S_B|} \quad (11)$$

where  $S_A, S_B$  are two segmentations by different approaches.

In addition, Jacobian determinant was employed to measure the smoothness of transformation. Under the same registration accuracy, higher minimum Jacobian and lower maximum one indicate better quality of transformation. To ensure diffeomorphism, Jacobian determinants of both  $\phi_1^{-v}$  and  $\phi_1^v$  were required to be above threshold 0.01 in this paper, which was achieved by tuning parameter  $\gamma_1$ .

### 3.2. Results on Circle-to-C shape registration

In this testing, two side matching with two-level hierarchical matching were employed to deform 'Circle' to 'C' shape image. Parameters were set as:  $\alpha = 0.01$ ,  $\gamma = 3$ ,  $\gamma_1 = 0.01$ , time unit 1/64. Fig. 1.a shows that the deformed circle by DMMS well recovered the 'C' shape, and one-one mapping under large deformation was achieved as illustrated by the regular deformed grids plotted in Fig. 1.b. Jacobian determinants were all positive, with minimum value 0.03, and the maximum one 20.

By comparison, the stationary-1<sup>st</sup>-order approach obtained worse quality deformed shape, with obscure recovery of the inner edges (see Fig. 1.a). Its parameter setting was the same as DMMS, except that  $\gamma_1$  was set to 0.8 to satisfy Jacobian threshold.

### 3.3. Results on synthesized brain image registration

In this category, DMMS was compared against other stationary and non-stationary approaches. All methods adopted one-side matching functional. For DMMS, stationary-integral and stationary-1<sup>st</sup>-order methods, the scaling and squaring procedure adopted time unit 1/32 during gradient computation, and 1/16 during line search. For stationary-integral approach, the gradient computation was based on 8 uniformly sampled time points. Eight time steps were also used in LDDMM. Both stationary and non-stationary methods shared the same parameter settings:  $\alpha = 0.01$ ,  $\gamma = 3$ ; four-level coarse-to-fine registration scheme; the stopping criterion  $\epsilon_1$  in (9) set to  $10^{-6}$ , and maximum 100 iterations allowed at the finest level. Conjugate method was employed to accelerate the convergence. Parameter  $\gamma_1$  was tuned for each method to satisfy Jacobian threshold (0.01), and single parameter was applied to all images.

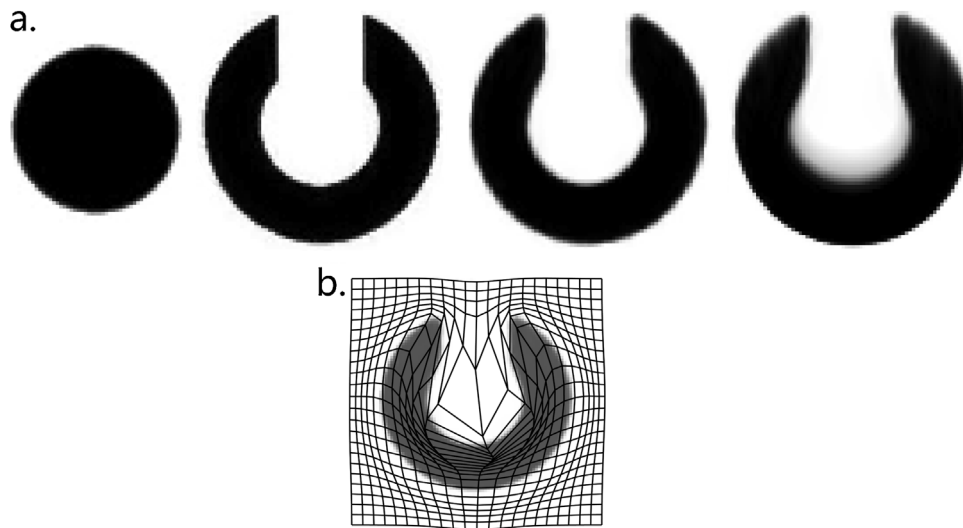


**Fig. 1.** Circle-to-C shape deformation results. Panel a, from left to right: ‘Circle’ image (size  $94 \times 92$ ), ‘C’ shape image, deformed ‘Circle’ by DMMS, deformed ‘Circle’ by stationary-1<sup>st</sup>-order approach; Panel b: deformation field by DMMS.

**Table 1**

Comparison of DMMS and several other brain registration methods on synthesized brain images. Each row represents one pair of images, and the order keeps the same for different approaches.  $J$  denotes Jacobian determinant.

	White matter (Dice)	Gray matter (Dice)	CSF (Dice)	$J_{\min} / J_{\max}$
DMMS	0.8278	0.8229	0.7106	0.023/24.9
$\gamma_1 = 0.18$	0.8255	0.8183	0.684	0.03/14.7
	0.8352	0.8306	0.6775	0.051/11.1
	0.8324	0.8318	0.7199	0.03/16.5
	0.8332	0.8210	0.6567	0.04/19.3
	0.7986	0.7991	0.6422	0.029/19.9
Stationary- integral	0.8269	0.8225	0.7092	0.026/21.9
$\gamma_1 = 0.18$	0.8232	0.8166	0.6823	0.014/15.7
	0.8358	0.8307	0.6777	0.025/17.3
	0.8315	0.8314	0.7199	0.018/18.6
	0.8338	0.8214	0.6620	0.023/26.6
	0.7966	0.7978	0.6414	0.04/15.8
Stationary-1 <sup>st</sup> - order	0.8021	0.7988	0.6873	0.063/10.0
$\gamma_1 = 0.35$	0.801	0.7979	0.6624	0.1/8.6
	0.8056	0.8028	0.6537	0.011/22.9
	0.8083	0.8105	0.7017	0.09/8.5
	0.8064	0.7949	0.6356	0.02/5.6
	0.7761	0.7789	0.6228	0.054/14.5
LDDMM	0.8188	0.8152	0.7046	0.05/20
$\gamma_1 = 0.47$	0.8211	0.8153	0.6824	0.013/13.5
	0.8204	0.8171	0.6677	0.079/11.7
	0.8248	0.8256	0.7165	0.054/12.1
	0.8217	0.8101	0.6488	0.09/14.8
	0.7912	0.7928	0.6375	0.072/11.4
Diffeomorphic Demons	0.802	0.794	0.656	-4.66/13.0
	0.804	0.792	0.630	-4.42/15.2
	0.808	0.795	0.576	-4.32/11.1
	0.818	0.813	0.686	-5.42/10.6
	0.814	0.7891	0.5208	-8.82/21.5
	0.7705	0.7690	0.5988	-12.0/21.1

LDDMM: large deformation diffeomorphic metric mapping.

DMMS: diffeomorphic mapping using stationary velocity (the proposed method).

Stationary-integral: stationary approach adopting integral form of gradient.

Stationary-1st-order: stationary approach adopting first order approximation for gradient.

Gaussian kernel parameters for diffeomorphic demons were set as:  $\sigma_{fluid} = 1$ ,  $\sigma_{diffuse} = 1$ , maximum step allowed be 2.5. Coarse-to-fine strategy was also adopted, and the stopping criteria were the same as DMMS.

Accuracy by these methods is shown in Table 1. The dices by DMMS and stationary-integral method were almost the same,

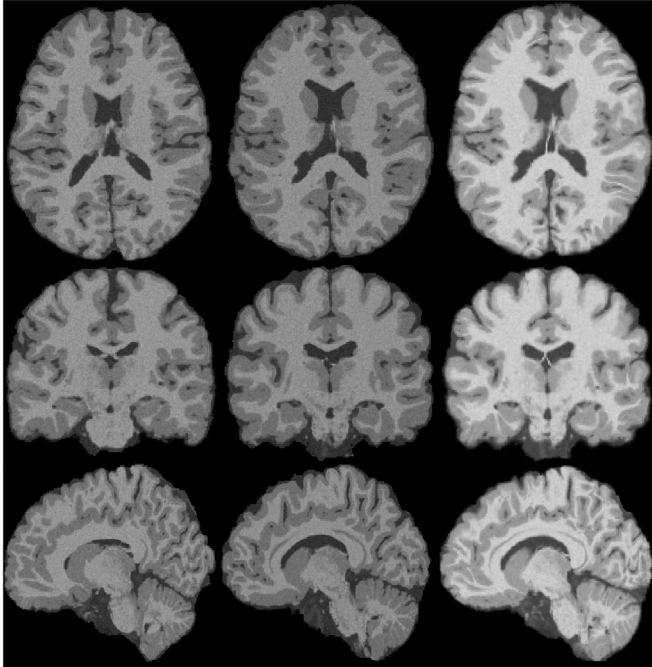
almost around 0.82 on white/gray matters, and 0.7 on CSF. From Fig. 2, we can see that nonlinear warping by DMMS significantly bridged the inter-subject morphological variations, especially for the subcortical regions. Dices by stationary-1<sup>st</sup>-order were 2~3% lower than DMMS. LDDMM reached the Jacobian threshold at higher  $\gamma_1$  (0.47), and under this setting, it did not demonstrate higher accuracy than DMMS, and its results at lower  $\gamma_1$  can be found in supplemental information online. Dices by demons were close to those by stationary-1<sup>st</sup>-order method, almost around 0.8 on gray/white matters (see Table 1), and there were negative Jacobian determinants, which was consistent with the results reported in literatures [31]. In fact, we also tested another stationary approach, DARTEL provided in SPM package using the parameters suggested before [28], but did not find higher accuracy than demons. Details are not shown here.

Time complexity of these methods is shown in Table 2. It took DMMS 1.46 h to finish the registration of the volume ( $188 \times 152 \times 162$ ) on a 3.4 GHz CPU with dual cores, versus 2.05 h for stationary-integral, and 1.25 h for stationary-1<sup>st</sup>-order. The three methods only differ in gradient computation complexity, which is  $O(N)$  for stationary-integral, and  $O(\log_2 N)$  for DMMS and stationary-1st-order, where  $N$  is number of time sampling points. In terms of specific computational load, DMMS requires 10 interpolation operations on deformation field and/or images, versus 36 ones for stationary-integral and 6 ones for stationary-1<sup>st</sup>-order, and interpolations accounted for the main computational load. Time-varying approach had much more interpolations in both gradient computation (82) and end-point deformation generation (32), since displacement at each time required by the semi-Lagrange scheme was computed through iterative interpolations. As such, its running time on the volume ( $188 \times 152 \times 162$ ) was over 9 h. Diffeomorphic demons showed faster speed, terminating the process in 20 min. As to the memory load, the basic memory requirements for DMMS were about 1.52 G, versus 5.6 G for LDDMM.

### 3.4. Results on real brain image registration

Since the elderly brain images have large difference in brain position and size, the template was first affinely registered to 28 subjects using 12 dofs by FLIRT in FSL [33]. Before nonlinear registration, images were cropped with 2 voxel margin retained, and their variances were normalized to bridge the photometric variations.

a. synthesized image



b. real brain image

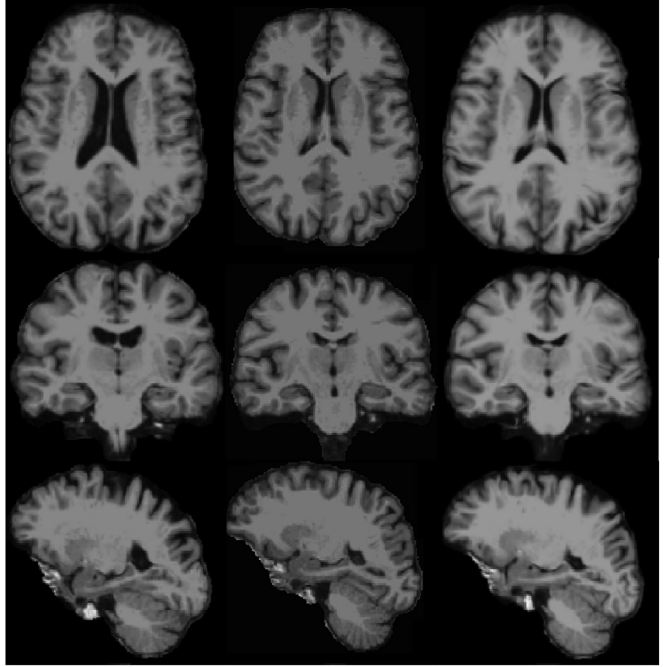


Fig. 2. Example of brain image deformation by DMMS. From left to right: template, target, deformed template.

**Table 2**  
Time complexity comparison between stationary and non-stationary approaches. Time cost was measured on volume size ( $188 \times 152 \times 162$ ) and 3.4GHz CPU with dual cores.

	DMMS	Stationary- integral	Stationary-1 <sup>st</sup> -order	LDDMM
Interpolations in gradient computation	10	36	6	82
Interpolations in $\phi_1$ generation	4	4	4	32
Tim cost for gradient computation	14.75 s	33.3 s	6.67 s	63.66
Tim cost for $\phi_1$ generation	3.79 s	3.79 s	3.79 s	25.61 s
Total running time	1.46 h	2.05 h	1.25 h	9.4 h

**Table 3**  
Comparison of DMMS and LDDMM on elderly brain image registration. Mean and standard deviation are shown for *dice*. For Jacobian determinants, the median, 1<sup>st</sup> and 3<sup>rd</sup> quartiles were shown.

	White matter ( <i>Dice</i> )	Cortical gray matter ( <i>Dice</i> )	Hippocampus ( <i>Dice</i> )	Cerebral spinal fluid ( <i>Dice</i> )	$J_{\min}$	$J_{\max}$
DMMS $\gamma_1 = 0.03$	0.806±0.02	0.653±0.014	0.767±0.038	0.88±0.038	0.09 (0.06,0.12)	8.5 (6.8,11.8)
LDDMM $\gamma_1 = 0.04$	0.804±0.02	0.65±0.015	0.765±0.039	0.879±0.039	0.11 (0.07,0.13)	8.7 (6.8,14.0)

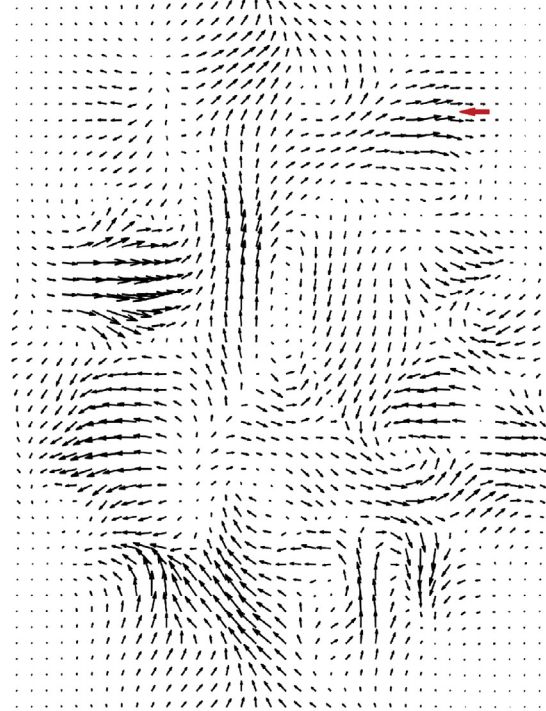
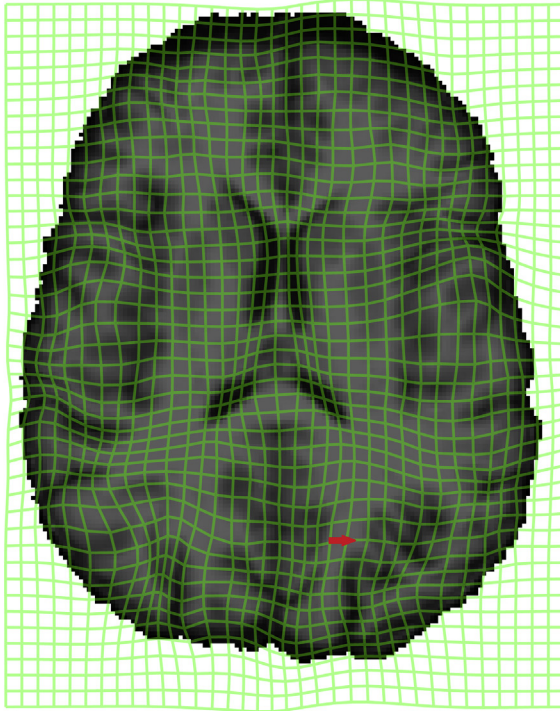
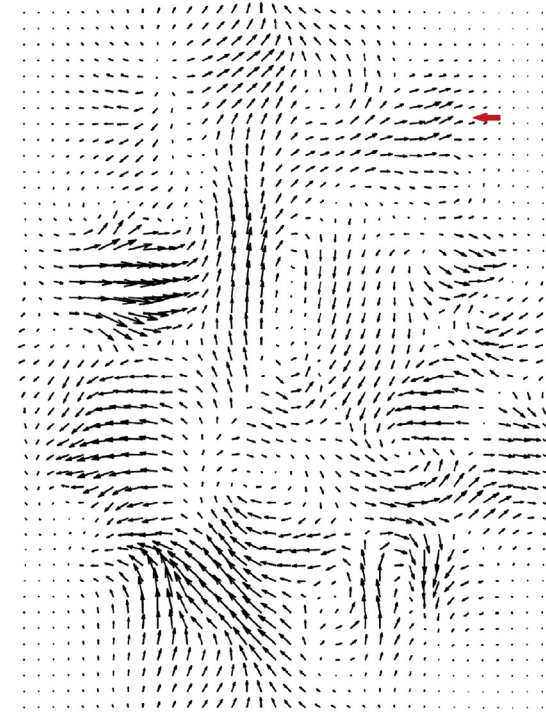
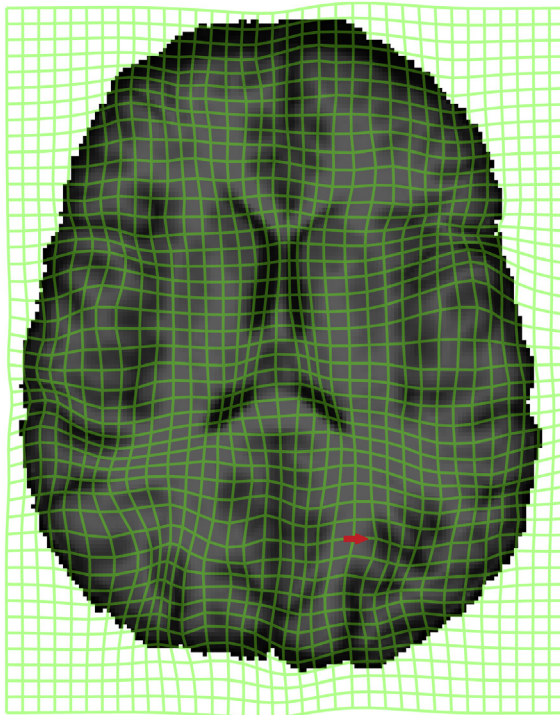
In this category, we focus on the evaluation between DMMS and LDDMM. The experimental settings were the same as those on synthesized brain images, except that parameter  $\gamma_1$  was tuned to satisfy Jacobian threshold (0.01) for all 28 mappings, leading to  $\gamma_1 = 0.03$  for DMMS, and 0.04 for LDDMM. If  $\gamma_1$  was set to 0.03 for LDDMM, negative Jacobians began to appear. Statistical results are listed in Table 3. We can see that dices by the two approaches were very close on average, reaching about 0.805 on white matter, 0.65 on cortical gray matter, 0.77 on hippocampus, and 0.88 on CSF. No significant difference between the methods was found ( $p > 0.05$ ). Moreover, their Jacobian determinants were also within the same range. The plots in Fig. 2 demonstrated that large morphological variations between template and subject were greatly reduced after nonlinear warping by DMMS.

To further study characteristics of stationary and non-stationary approaches, their resulting deformation fields and velocity fields were plotted in Fig. 3. As we can see, the two approaches resulted in very similar deformation fields, and the stationary vector field

was very close to the time-varying one at  $t=0.5$ . The regular and consistent deformations at boundaries also reflected the treatment of the image volume as a closed domain, as can be observed from Fig. 1 as well. The plots in Fig. 4 showed that residuals by the two methods were similar, with 24.7% for DMMS, and 25% for LDDMM. But regularized energy by LDDMM ( $3.77 \times 10^9$ ) was smaller than DMMS ( $4.09 \times 10^9$ ), showing that time-varying parameterization will follow the shortest path, whereas stationary parameterization follows another one, specifically the group exponential path. Their optimization curves exhibits similar changing trend, and the inflection points on the curves indicated that the optimization actually corrected the 'over-registration' at coarser level.

#### 4. Discussion

In this paper, we have proposed a new simplified model for the optimal stationary velocity in diffeomorphic image registration, which is compact and effective. Compared with integral model, this

**(a) stationary****(b) non-stationary**

t=0.5

**Fig. 3.** Optimized deformation fields and vector fields by DMMS and LDDMM on the same elderly brain images. Projection on axial view is shown. Discrepancies between the two methods are indicated by red arrows.

single point model did not compromise brain mapping accuracy but reduce the complexity a lot. Although both approaches have same complexity for end-point transformation generation, the gradient computation complexity for integral model is  $O(N)$ , versus  $O(\log_2 N)$

for the proposed model, where  $N$  is number of time sampling points. As such, this approach can save the time cost by more than 30 min, reaching about 1.5 h for a typical brain registration task on a 3.4 GHz dual core CPU, and the speed can be further improved on GPU

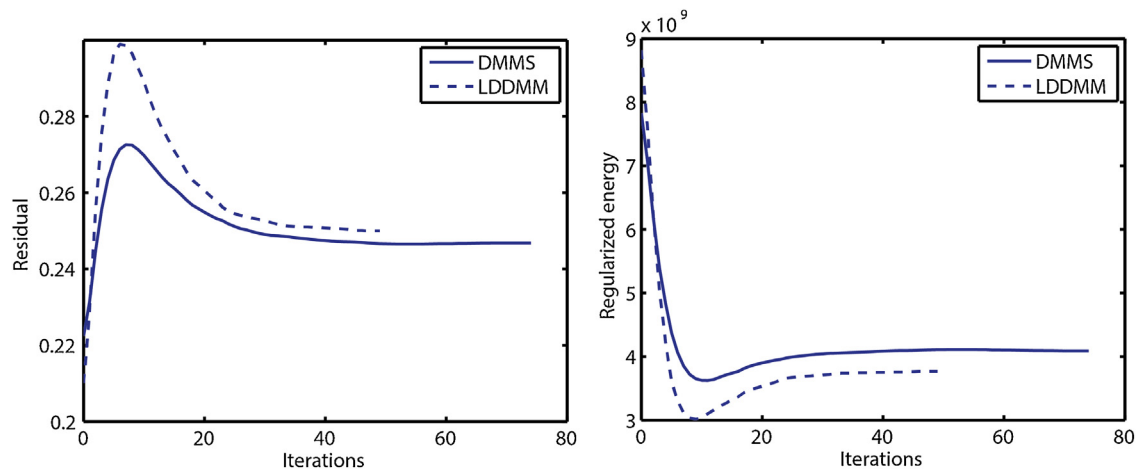


Fig. 4. Optimization curves at the finest level for registration task shown in Fig. 3.

[34]. This model also showed clear advantage over the first order approximation model in handling large deformation and achieved comparable speed. Validity of this model comes from the smoothness of transformation based on which mean value theorem of definite integral is satisfied. Here we need to clarify that this model differs from the symmetric registration model (SyN) [19] because SyN measures the cost function at middle time point, whereas in ours the middle time point only appears in the solution, and it is just a special case of derivation. By comparing with other stationary approaches, e.g. diffeomorphic demons, we found that DMMS demonstrated higher accuracy and smoother transformation.

By extensive comparison with time-varying approach LDDMM on both synthesized and real brain images, we found that DMMS could achieve comparable brain mapping performance with much faster speed. The complexity of non-stationary approach is  $O(N)$  for generating end-point transformation as well as gradient computation, whereas that for DMMS is  $O(\log_2 N)$ . It was shown that DMMS could tolerate smaller regularization parameter to satisfy positive Jacobian threshold. From theoretical analysis, time-varying parameterization can deform the space more freely, hence larger regularization parameter is required to resist those non-smooth deformations. Moreover, grids system resolution also limits the accuracy of time-varying parameterization though theoretically it covers larger solution space. As a result, these factors made the accuracy by stationary and non-stationary approaches comparable in practice. It is also worth mentioning that in this work we just applied a single regularization parameter to all tasks, but did not tune it for individual images, so accuracy on some images may be under-estimated. But this criterion was applied to both DMMS and LDDMM, so the method comparison was fair.

Through experiment, we also observed intrinsic links between stationary and non-stationary parameterizations. For instance, the stationary vector field is very similar to the time-varying one at middle time point, and similarity holds for their deformation fields and optimization curves, despite that their implementations were significantly different. These evidences proved efficacy of the proposed method and indicate its promising application in brain mapping tasks where LDDMM achieved success.

We also noted that, however, cortical registration purely based on gray level information could not result in accurate cortical alignment, as can be observed from Fig. 2. Previous researches have shown that incorporating landmarks, sulcal curves or surface information could significantly improve the cortical alignment accuracy [35–37], so it will be interesting to apply such multi-modality matching on DMMS to see if the accuracy limit could be broken without violating the diffeomorphism constraint. It will be also

interest to incorporate learning approach [38,39] to improve the registration performance on specific dataset. Here we should point out that this method is a general registration approach without making assumptions on brain anatomies, hence it can be easily adapted to images of other organs.

## 5. Conclusion

In conclusion, the proposed method is shown to effectively reduce the complexity of stationary velocity based diffeomorphic metric mapping while achieving registration accuracy and transformation smoothness similar to non-stationary approach, which exposes promising application in large scale brain manifold analysis.

## Acknowledgments

This work was supported by the National Science Fund of China under Grant Nos. 81771915, U1713208, 61472187, 61602444 and Start-Up Research Fund at Nanjing University of Science & Technology. The authors would like to thank BrainWeb and Alzheimer's Disease Neuroimaging Initiative (ADNI) for data collection and sharing.

## Appendix A. Supplementary data

Supplementary material related to this article can be found, in the online version, at doi:<https://doi.org/10.1016/j.jocs.2018.11.011>.

## References

- [1] X. Pennec, *Statistical Computing on Manifolds: From Riemannian Geometry to Computational Anatomy*, Emerg. Trends Visual Comput. 5416 (2009) 347–386.
- [2] J. Ashburner, K.J. Friston, *Voxel-based morphometry—the methods*, Neuroimage 11 (6 Pt 1) (2000) 805–821.
- [3] U. Grenander, M.I. Miller, *Pattern Theory: From Representation to Inference*, Oxford University Press, Oxford, 2007, xii, 596 p.
- [4] S. Joshi, et al., *Unbiased diffeomorphic atlas construction for computational anatomy*, Neuroimage 23 (Suppl 1) (2004) S151–60.
- [5] H.Z. Wang, et al., *Multi-atlas segmentation with joint label fusion*, IEEE Trans. Pattern Anal. Mach. Intell. 35 (3) (2013) 611–623.
- [6] K.J. Friston, et al., *Statistical Parametric Mapping: The Analysis of Functional Brain Images*, Academic Press, 2007.
- [7] M.F. Beg, et al., *Computing large deformation metric mappings via geodesic flows of diffeomorphisms*, Int. J. Comput. Vis. 61 (2) (2005) 139–157.
- [8] M.I. Miller, A. Trounev, L. Younes, *On the metrics and euler-lagrange equations of computational anatomy*, Annu. Rev. Biomed. Eng. 4 (2002) 375–405.

- [9] S.C. Joshi, M.I. Miller, Landmark matching via large deformation diffeomorphisms, *IEEE Trans. Image Process.* 9 (8) (2000) 1357–1370.
- [10] J. Glaunes, et al., Large deformation diffeomorphic metric curve mapping, *Int. J. Comput. Vis.* 80 (3) (2008) 317–336.
- [11] J. Du, A. Goh, A. Qiu, Large deformation diffeomorphic metric mapping of orientation distribution functions, *Inf. Process. Med. Imaging* 22 (2011) 448–462.
- [12] M. Vaillant, J. Glaunes, Surface matching via currents, *Inf. Process. Med. Imaging* 19 (2005) 381–392.
- [13] M.I. Miller, et al., Collaborative computational anatomy: an MRI morphometry study of the human brain via diffeomorphic metric mapping, *Hum. Brain Mapp.* 30 (7) (2009) 2132–2141.
- [14] L. Wang, et al., Large deformation diffeomorphism and momentum based hippocampal shape discrimination in dementia of the Alzheimer type, *IEEE Trans. Med. Imaging* 26 (4) (2007) 462–470.
- [15] A. Qiu, M.I. Miller, Multi-structure network shape analysis via normal surface momentum maps, *Neuroimage* 42 (4) (2008) 1430–1438.
- [16] X. Yang, et al., Evolution of hippocampal shapes across the human lifespan, *Hum. Brain Mapp.* 34 (11) (2013) 3075–3085.
- [17] X. Yang, M.Z. Tan, A. Qiu, CSF and brain structural imaging markers of the Alzheimer's pathological cascade, *PLoS One* 7 (12) (2012), p. e47406.
- [18] L.S. Lim, et al., Variations in eye volume, surface area, and shape with refractive error in young children by magnetic resonance imaging analysis, *Invest. Ophthalmol. Vis. Sci.* 52 (12) (2011) 8878–8883.
- [19] B.B. Avants, et al., Symmetric diffeomorphic image registration with cross-correlation: evaluating automated labeling of elderly and neurodegenerative brain, *Med. Image Anal.* 12 (1) (2008) 26–41.
- [20] J. Ashburner, K.J. Friston, Diffeomorphic registration using geodesic shooting and Gauss-Newton optimisation, *Neuroimage* 55 (3) (2011) 954–967.
- [21] A. Mang, L. Ruthotto, A Lagrangian Gauss-Newton-Krylov Solver for Mass- and Intensity-Preserving Diffeomorphic Image Registration, *Siam J. Sci. Comput.* 39 (5) (2017) B860–B885.
- [22] M. Zhang, P. Fletcher, Finite-dimensional lie algebras for fast diffeomorphic image registration, *Inf. Process. Med. Imaging* (2015) 249–260.
- [23] F.X. Vialard, et al., Diffeomorphic 3D Image Registration via Geodesic Shooting Using an Efficient Adjoint Calculation, *Int. J. Comput. Vis.* 97 (2) (2012) 229–241.
- [24] V. Arsigny, et al., A log-Euclidean framework for statistics on diffeomorphisms, *Med. Image Comput. Comput. Assist. Interv.* 9 (Pt 1) (2006) 924–931.
- [25] M. Lorenzi, X. Pennec, Geodesics, Parallel transport & one-parameter subgroups for diffeomorphic image registration, *Int. J. Comput. Vis.* 105 (2) (2013) 111–127.
- [26] T. Vercauteren, et al., Symmetric log-domain diffeomorphic Registration: a demons-based approach, *Med. Image Comput. Comput. Assist. Interv.* 11 (Pt 1) (2008) 754–761.
- [27] M. Hernandez, M.N. Bossa, S. Olmos, Registration of anatomical images using paths of diffeomorphisms parameterized with stationary vector field flows, *Int. J. Comput. Vis.* 85 (3) (2009) 291–306.
- [28] J. Ashburner, A fast diffeomorphic image registration algorithm, *Neuroimage* 38 (1) (2007) 95–113.
- [29] M. Bossa, et al., Tensor-based morphometry with stationary velocity field diffeomorphic registration: application to ADNI, *Neuroimage* 51 (3) (2010) 956–969.
- [30] X. Yang, et al., Diffeomorphic metric landmark mapping using stationary velocity field parameterization, *Int. J. Comput. Vis. Image Process.* 115 (2) (2015) 69–86.
- [31] T. Vercauteren, et al., Diffeomorphic demons: efficient non-parametric image registration, *Neuroimage* 45 (1 Suppl) (2009) S61–72.
- [32] B. Fischl, et al., Whole brain segmentation: automated labeling of neuroanatomical structures in the human brain, *Neuron* 33 (3) (2002) 341–355.
- [33] S.M. Smith, et al., Advances in functional and structural MR image analysis and implementation as FSL, *Neuroimage* 23 (2004) S208–S219.
- [34] Y.D. Zhang, et al., Multiple sclerosis identification by convolutional neural network with dropout and parametric ReLU, *J. Comput. Sci.* 28 (2018) 1–10.
- [35] J. Du, L. Younes, A.Q. Qiu, Whole brain diffeomorphic metric mapping via integration of sulcal and gyral curves, cortical surfaces, and images, *Neuroimage* 56 (1) (2011) 162–173.
- [36] A.A. Joshi, et al., Surface-constrained volumetric brain registration using harmonic mappings, *IEEE Trans. Med. Imaging* 26 (12) (2007) 1657–1669.
- [37] G. Postelnicu, L. Zollei, B. Fischl, Combined Volumetric and surface registration, *IEEE Trans. Med. Imaging* 28 (4) (2009) 508–522.
- [38] S.H. Wang, et al., Polarimetric synthetic aperture radar image segmentation by convolutional neural network using graphical processing units, *J. Real. Image Process.* 15 (3) (2018) 631–642.
- [39] Y.D. Zhang, et al., Abnormal breast identification by nine-layer convolutional neural network with parametric rectified linear unit and rank-based stochastic pooling, *J. Comput. Sci.* 27 (2018) 57–68.



**Xianfeng Yang** received the PhD degree from University of Queensland, on the subject of biomedical imaging analysis in 2015. He has been an associate professor at School of Computer Science and Engineering, Nanjing University of Science and Technology since 2017. He had research experience at Queensland Brain Institute, National University of Singapore and Institute of Automation, CAS in neuroscience field. His research interests include MRI analysis, brain networks and imaging genetics.



**Jian Yang** received the PhD degree from Nanjing University of Science and Technology (NUST), on the subject of pattern recognition and intelligence systems in 2002. In 2003, he was a postdoctoral researcher at the University of Zaragoza. From 2004 to 2006, he was a Postdoctoral Fellow at Biometrics Centre of Hong Kong Polytechnic University. From 2006 to 2007, he was a Postdoctoral Fellow at Department of Computer Science of New Jersey Institute of Technology. Now, he is a Chang-Jiang professor in the School of Computer Science and Technology of NUST. He is the author of more than 100 scientific papers in pattern recognition and computer vision. His journal papers have been cited more than 4000 times in the ISI Web of Science, and 9000 times in the Web of Scholar Google. His research interests include pattern recognition, computer vision and machine learning. Currently, he is/was an associate editor of Pattern Recognition Letters, IEEE Trans. Neural Networks and Learning Systems, and Neurocomputing. He is a Fellow of IAPR.